THE JOURNAL OF BIOLOGICAL CHEMISTRY VOL. 291, NO. 37, pp. 19462–19473, September 9, 2016

Structural Plasticity of Cholesteryl Ester Transfer Protein Assists the Lipid Transfer Activity*[S]

Received for publication, June 22, 2016, and in revised form, July 20, 2016 Published, JBC Papers in Press, July 20, 2016, DOI 10.1074/jbc.M116.744623

Venkat R. Chirasani, Prasanna D. Revanasiddappa, and Sanjib Senapati[1]

From the Bhupat and Jyoti Mehta School of Biosciences and Department of Biotechnology, Indian Institute of Technology Madras, Chennai 600036, India

Cholesteryl ester transfer protein (CETP) mediates the transfer of cholesteryl esters (CEs) and triglycerides between different lipoproteins. Recent studies have shown that blocking the function of CETP can increase the level of HDL cholesterol in blood plasma and suppress the risk of cardiovascular disease. Hence, understanding the structure, dynamics, and mechanism by which CETP transfers the neutral lipids has received tremendous attention in last decade. Although the recent crystal structure has provided direct evidence of the existence of strongly bound CEs in the CETP core, very little is known about the mechanism of CE/triglyceride transfer by CETP. In this study, we explore the large scale dynamics of CETP by means of multimicrosecond molecular dynamics simulations and normal mode analysis, which provided a wealth of detailed information about the lipid transfer mechanism of CETP. Results show that the bound CEs intraconvert between bent and linear conformations in the CETP core tunnel as a consequence of the high degree of conformational flexibility of the protein. During the conformational switching, there occurred a significant reduction in hydrophobic contacts between the CEs and CETP, and a continuous tunnel traversing across the CETP long axis appeared spontaneously. Thus, our results support the recently proposed "tunnel mechanism" of CETP from cryo-EM studies for the transfer of neutral lipids between different lipoproteins. The detailed understanding obtained here could help in devising methods to prevent CETP function as a cardiovascular disease therapeutic.

Coronary heart disease (CHD)[2] is one of the prime causes of an increase in the mortality rate worldwide. Over the past few years, various epidemiological studies have provided ample evidence that increased levels of HDL, by transporting cholesterol from atherosclerotic plaques to liver for excretion, can arrest the progression of CHD (1, 2). Subsequent preclinical studies on overexpression of apolipoprotein A-I (apoA-I), the major protein constituent of HDL, have reported significant reduction in CHD risk (3, 4). Although raising HDL levels is a long-standing strategy for mitigating CHD risk, the current lipid-targeted therapies, including the usage of statins, fibrates, and niacin, have shown reduced therapeutic potential (5–7). Hence, there is a continuous requirement for new strategies that can elevate HDL levels to halt the progression of CHD.

Cholesteryl ester transfer protein (CETP), a plasma glycoprotein with 476 residues, has been found to mediate the transfer of cholesteryl esters (CEs) from HDL to LDL and VLDL as well as the reciprocal transfer of triglycerides (TGs) from LDL and VLDL to HDL (8, 9). The identification of deficient CETP gene levels and correlated high HDL levels in a Japanese population (10–13) brought CETP into focus as a therapeutic target for controlling HDL levels. Preclinical animal model studies have further substantiated these findings by showing an elevated level of HDL in mice with non-expressing CETP (14–16). Since then, the inhibition of CETP activity by small molecule inhibitors has been pursued as an active approach to prevent atherosclerosis with varying levels of success at clinical trial phases (17–20). Given the complexity of lipid metabolism and the pivotal role of CETP in the process, understanding CETP structure, CETP inhibition, and the mechanism by which CETP transfers neutral lipids is of prime importance. The last decade, therefore, has seen the employment of sophisticated techniques, like cryo-EM (21, 22), x-ray (23, 24), and MD simulations (25–28) on this front. Nevertheless, the story of CETP remains far from complete.

The crystal structure of CETP (Protein Data Bank entry 2OBD) has been solved with four bound lipid molecules (23). The structure shows two β-barrel domains at the N and C termini, each with a twisted β-sheet and a long α-helix; a central β-sheet between the two β-barrels; a C-terminal α-helix; and a 60-Å-long hydrophobic tunnel occupied by two CE molecules. Additionally, there were two plug-in dioleoylphosphatidylcholine molecules with polar headgroups exposed to plasma and acyl chains buried in the hydrophobic tunnel of CETP. Interestingly, one of the CEs in the hydrophobic tunnel was in the bent conformation, whereas the second CE molecule was in the linear conformation. Recent cryopositive staining EM and optimized negative-staining electron microscopy (OpNS-EM) protocols combined with CETP C terminus-specific polyclonal antibody studies have suggested that CETP penetrates its C-terminal β-barrel domain into LDL or VLDL and its N-terminal β-barrel domain into HDL to form a ternary complex (21). Further, it was suggested that the aforementioned long continuous hydrophobic tunnel that traverses along the long axis of CETP can connect to the core of HDL and LDL simultaneously to facilitate the transfer of CEs and TGs between the lipoproteins.

* The authors declare that they have no conflicts of interest with the contents of this article.

[S] This article contains supplemental Table 1 and Figs. S1–S7.

[1] To whom correspondence should be addressed. Tel.: 91-44-2257-4122; Fax: 91-44-2257-4102; E-mail: sanjibs@iitm.ac.in.

[2] The abbreviations used are: CHD, coronary heart disease; CETP, cholesteryl ester transfer protein; CE, cholesteryl ester; MD, molecular dynamics; NMA, normal mode analysis; PL, phospholipid; COM, center of mass; ANMA, anisotropic network model analysis.

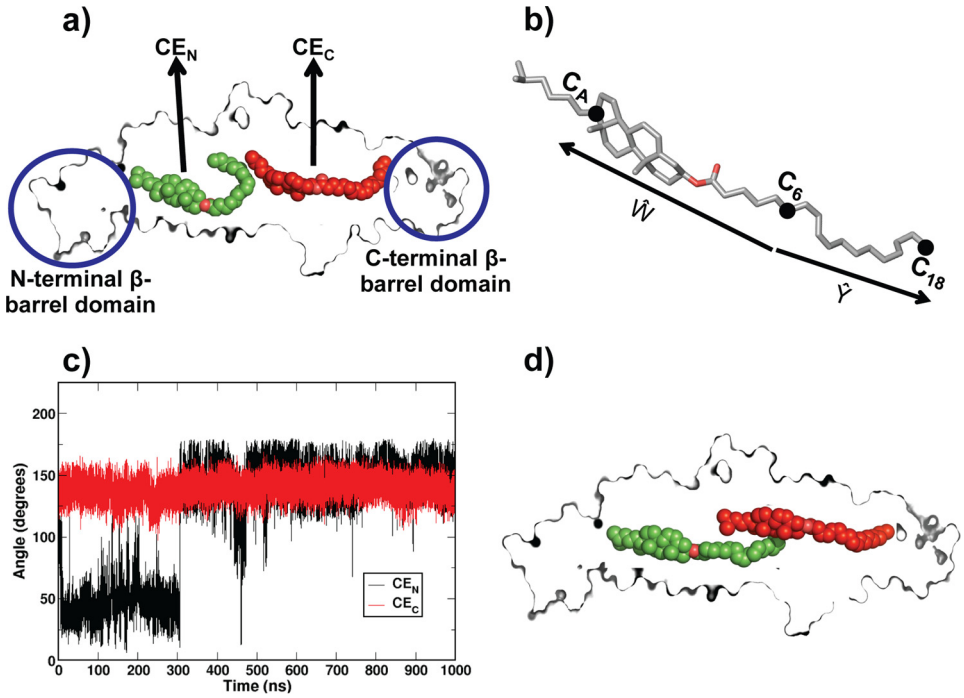

FIGURE 1. **Conformational switching of bound CEs in CETP.** *a*, conformation of the CEs in CETP crystal structure. Two bound CEs are named CE_N (*green*) and CE_C (*red*) and shown in a van der Waals representation. CETP is shown in sliced surface mode. *b*, molecular structure of CE. Two vectors, $\hat{W}$ and $\hat{Y}$, directed from C_6 to C_A and from C_6 to C_{18} atoms are defined to measure the oleate angle. *c*, time evolution of the CE oleate angle from CETP crystal structure simulation (system 1 in supplemental Table S1). Results are shown for both CE_N (*black*) and CE_C (*red*). *d*, a representative linear conformation of the CEs in CETP tunnel at 1 μs of simulation time.

Thus, crystal structure has provided a wealth of information about the structure of CETP and the nature of binding of CEs in CETP. However, due to the inherent limitations of the technique, a dynamic phenomenon, such as the time evolution of the protein conformation and its bound substrates, CEs, could not be captured. State-of-the-art molecular dynamics (MD) simulations can capture short to large scale dynamic processes by mapping the interatomic interactions at a resolution as high as 1 fs. Hence, in this study, we have employed multimicrosecond-long atomistic simulations to explore the dynamics of CETP and its bound substrates and to understand the mechanism of lipid transfer by CETP. We have observed high degrees of conformational flexibility of CETP and bound CEs as well as the frequent interconversion of the CEs between the bent and linear conformations, which resulted in the formation of a continuous hydrophobic tunnel spanning the length of CETP.

Results and Discussion

In MD simulations, it is important to ensure that the system is well equilibrated before analyzing the simulation trajectory. A simple strategy is to monitor the mean square displacements of the protein residues from their initial positions. Hence, we plotted the time evolution of the root mean square displacements of C_α atoms of CETP, which is shown in supplemental Fig. S1. The figure depicts the convergence of root mean square displacements only at 130 ns, demonstrating the necessity of long simulation for equilibration. In fact, such a long simulation time is expected, considering the large molecular size of CETP and the intrinsic dynamics of bound lipid molecules in CETP. However, once equilibrated, CETP maintained stability throughout the simulation.

CETP-bound CE Shows Conformational Switching in Nano- to Microsecond Time Scales—Although CETP displayed considerable stability after equilibration, visual inspection of simulation trajectory revealed an interesting conformational switching of the core lipids, CEs, in the hydrophobic tunnel of CETP. Particularly, the N-terminal CE, CE_N, exhibited frequent interswitching between the bent and linear conformations, although the C-terminal CE, CE_C, maintained a linear conformation throughout the 1-μs simulation run. Recall that in the solved CETP crystal structure, CE_N was in the bent conformation, whereas CE_C was in the linear form, as shown in Fig. 1*a*. We will elaborate on this transition of CEs below. It was also evident from the visual inspection that the change in conformation of CE_N was effected through the flexibility of oleate chain, whereas the cholesterol moiety maintained a high degree of rigidity. To locate precisely the pivot of CE_N bending, we computed the gauche/trans ratio of each dihedral angle in the oleate chain of CE_N (supplemental Fig. S2*a*). For higher accuracy, we divided the whole trajectory into two parts: (*a*) frames with CE_N in the bent conformation and (*b*) frames with CE_N in the linear conformation. Subsequently, we calculated the average fraction of gauche defects for each dihedral angle present in the oleate chain of CE_N in both frames. As a control, we also analyzed the gauche fraction in the dihedrals of the oleate chain of CE_C. The dihedral angles in the oleate chain are numbered beginning with the C_1-C_2-C_3-C_4 fragment and ending with the C_{15}-C_{16}-C_{17}-C_{18} fragment, as shown in supplemental Fig. S2*a*. If the dihedral angle falls in the range 120°–240°, it is considered trans, the remainder being gauche (29). From the plotted distributions of dihedral angles in supplemental Fig. S2*b*, it is evi-

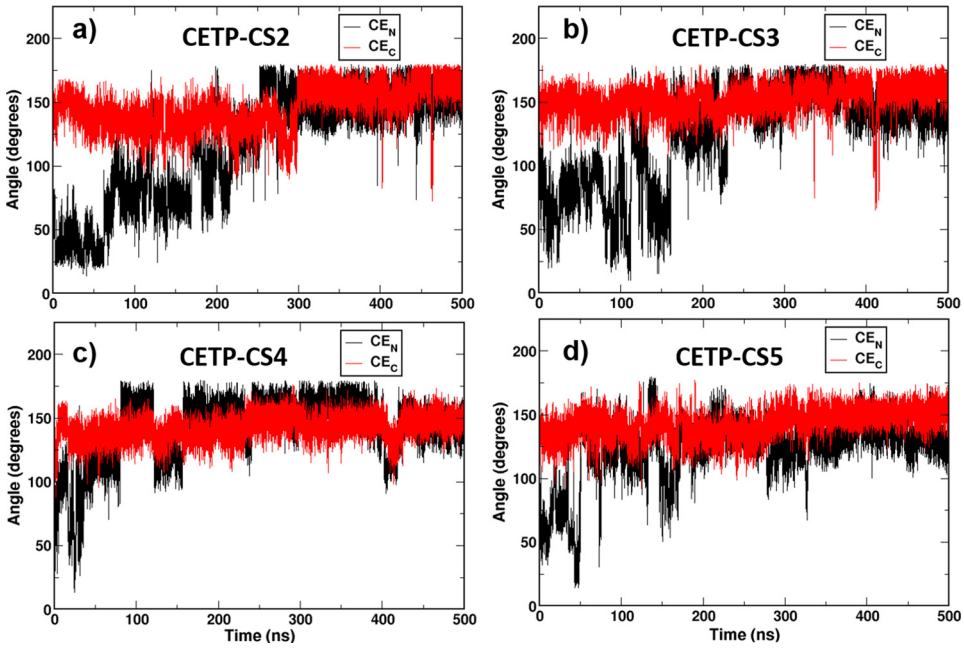

FIGURE 2. **Conformational switching of bound CEs in the replica simulations of CETP crystal structure.** Time evolutions of the oleate angle of CE_N (*black*) and CE_C (*red*) are shown in the replica systems: CETP-CS2 (*a*), CETP-CS3 (*b*), CETP-CS4 (*c*), and CETP-CS5 (*d*). For system definition, see supplemental Table S1.

dent that the dihedral angle III (C_3-C_4-C_5-C_6) and dihedral angle V (C_5-C_6-C_7-C_8) in the oleate chain of bent CE_N prefer the gauche conformation, whereas the same dihedral angles in CE_C and linear CE_N oleate chains prefer the trans conformation. Hence, the shift in dihedral angles III and V from gauche to trans is responsible for conformational switching of CE_N between bent and linear.

Thus, from the gauche fraction of the dihedral angles in the CE_N oleate chain, we were able to identify the most flexible region in CE. We specifically found dihedral angle V to exhibit the largest difference in the gauche fraction in the bent CE conformation compared with the linear CE conformation. Further, to determine the extent of bending in CE_N, we took C_6 of dihedral angle V as the central node to calculate the angle between the oleate chain and cholesterol ring of CE. The angle was estimated by computing the instantaneous angle assumed by two vectors, $\hat{W}$ and $\hat{Y}$, drawn on the molecular frames. The vector from C_6 to C_A of the cholesterol ring moiety was termed $\hat{W}$, and the one from C_6 to the oleate chain's terminal carbon C_{18} was termed $\hat{Y}$ (Fig. 1*b*). The angle between the two vectors, termed the oleate angle, was then computed as follows.

$$\theta = \cos^{-1}(\hat{W}.\hat{Y}/|\hat{W}||\hat{Y}|) \qquad \text{(Eq. 1)}$$

In order to understand the frequency of CE conformational switching between the bent and linear conformations, we plotted the computed angle against simulation time, as shown in Fig. 1*c*. The intermittent switching of CE_N between the bent and linear conformations was evident. For example, at 305 ns of simulation time, CE_N transformed to an extended conformation that was very similar to CE_C. Interestingly, this extended conformation lasted for about 170 ns and again adopted back the bent conformation for about 5 ns. After this brief spell of the bent conformation, CE_N reverted to a stable linear conformation for rest of the simulation time, as shown in Fig. 1*c*. Although CE_N was flexible in switching conformations between bent and linear, CE_C remained in the straight conformation. The extended linear conformations, as attained by both CE_N and CE_C in the CETP hydrophobic tunnel during the later phase of simulation (0.45–1 μs), are shown in Fig. 1*d*.

To strengthen our findings of frequent conformational switching of CE_N in the CETP tunnel, we performed a new set of MD simulations on the same CE-bound CETP crystal structure but with a different set of initial velocities of the constituent atoms chosen randomly from a Maxwell-Boltzmann distribution (supplemental Table S1). Conformational switching of CE_N was again characterized by calculating the bending angle of the CE oleate chain, as discussed above. Interestingly, all of these replica simulations have displayed significant flexibility in CE_N conformation despite the stable and linear CE_C conformation (Fig. 2). More importantly, CE_N interswitches between the bent and linear conformations, very similar to those of the primary system, CETP-CS1. However, the switching time and frequency of CE_N varies from system to system due to their different initial conditions. For example, whereas systems 2 and 3 required a prolonged 200–300-ns simulation time to transform CE_N from bent to linear, system 4 does it rather quickly in about 100 ns. The conformational transition of CE_N in system 5 is most interesting, where the lipid exhibits a back-and-forth motion between the two conformations during the first 200 ns and then settles to the linear conformation at a longer time. Thus, in solution, the bound CE_N in the CETP tunnel interswitches between bent and linear conformations with a particular preference for the linear form.

Normal Mode Analysis Revealed More Frequent Conformational Switching of CE—As Figs. 1 and 2 indicate, the N-terminal CE of CETP has a tendency to shuttle between the bent and linear conformations. However, this transition appears to be somewhat restricted. One of the reasons could be the short

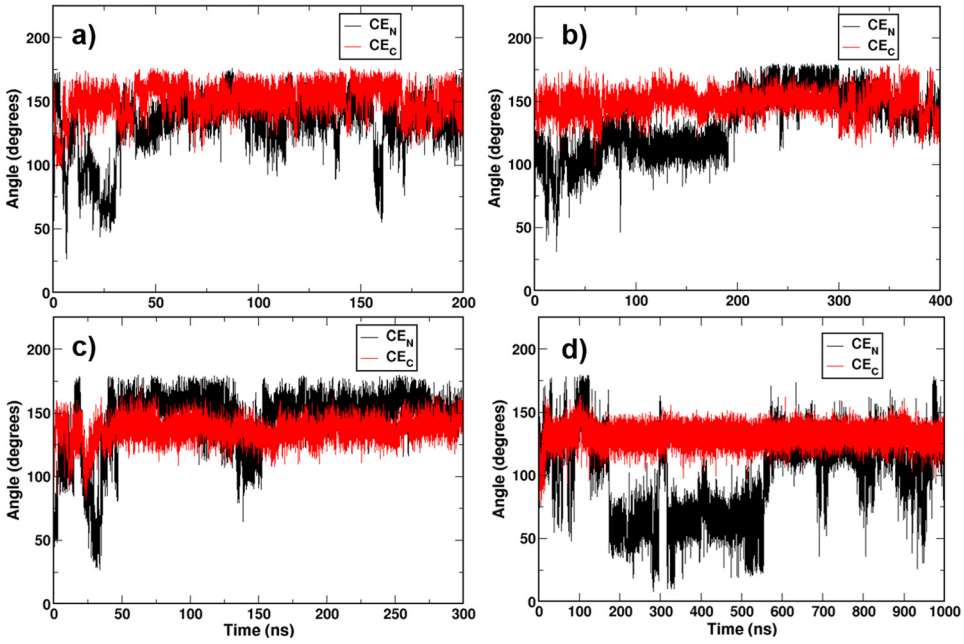

FIGURE 3. **Conformational switching of bound CEs in the MD simulations of NMA-derived relaxed CETP structures.** Time evolutions of the oleate angle of CE_N (*black*) and CE_C (*red*) are shown in the CETP-NM1 (*a*), CETP-NM2 (*b*), CETP-NM3 (*c*), and CETP-NM4 (*d*) systems. For system definition, see supplemental Table S1.

length and time scales covered under MD simulations. The changes that CETP undergoes in plasma and particularly when bound to lipoprotein would presumably be at much larger scales. To capture such large scale conformational changes, we performed normal mode analysis (NMA) on the CETP structure. NMA is a well tested time-dependent technique that identifies slow, large amplitude motions by investigating the low frequency vibrational modes of a protein described by an elastic network (30). From the NMA results, we extracted four CETP conformations that exhibited the largest variations from the CETP crystal structure. They were (*a*) normal mode 1 with CETP in an elongated or stretched conformation having a bending angle of 160°, named CETP-NM1 (bending angle in crystal structure 139°); (*b*) normal mode 2 with CETP in a curved conformation having a bending angle of 131°, named CETP-NM2; (*c*) normal mode 3 with the CETP N-terminal β-barrel domain torsionally twisted by ~15°, named CETP-NM3; and (*d*) normal mode 4 with both ~9° torsionally twisted N-terminal β-barrel domain and elongated CETP with a bending angle of 148°, named CETP-NM4. To see the conformational transitions of CEs in these NMA-generated CETP structures, we docked two CEs and two phospholipids (PLs) in each of these four structures and performed MD simulations for 200, 400, 300, and 1000 ns, respectively (supplemental Table S1). As Fig. 3 shows, the availability of a larger space in the core of CETP has allowed more frequent interconversion of CE_N between bent and linear conformations in these simulations on ANMA-generated structures. This was particularly evident in the CETP-NM4 system, where the bent to linear transition of CE_N was more frequent and periodic.

To better quantify the relative occurrences of the bent and linear conformations of CEs, we calculated the probability distributions of the CE oleate angle, $P(\theta)$, over the entire simulation trajectories, and the results are presented in Fig. 4. As the figure shows, the N-terminal CE in CETP shuttles between two major conformations, bent and linear, in all systems, suggesting that these two conformations can coexist. This is further supported by the simulation results from ANMA-generated CETP structures, particularly from CETP-NM4, which shows an almost equal propensity for the bent and linear conformations. The C-terminal CE, however, retains its native linear structure with a broad range of angle distribution between 120 and 180° in all systems. To summarize, the linear and bent conformations of CE in CETP coexist in solution. However, there is a particular preference for the linear conformation for both of the CEs in CETP relaxed structures, which might imply that CEs become linear for smooth transfer when CETP attaches to lipoproteins. We will elaborate on this hypothesis below.

Conformational Flexibility of CE Is Assisted by Bending and Twisting Motions of CETP—To investigate the possible reason behind the conformational flexibility of CEs and to see whether there is a correlation between CE conformational flexibility and CETP motions, we examined the distribution of bending and twisting angles in CETP. Fig. 5 shows the angular distributions of CETP from the simulation data. The bending motion was estimated by computing the angle between two vectors, $\hat{A}$ and $\hat{C}$. The vector from the center of mass (COM) of the central β-sheet to the COM of the N-terminal distal end was termed $\hat{A}$, and the other vector from the COM of the central β-sheet to the COM of the C-terminal distal end was termed $\hat{C}$. The angle subtended by these two vectors was computed using the same formula as in Equation 1.

From the angle distribution profile, it is evident that the CETP crystal structure undergoes significant conformational changes and can extend to a more linear conformation with the bending angle as high as 151° and bend to an arch-like conformation with a bending angle of 131° (the crystal structure angle is 139°), whereas relaxed CETP from NMA displayed relatively

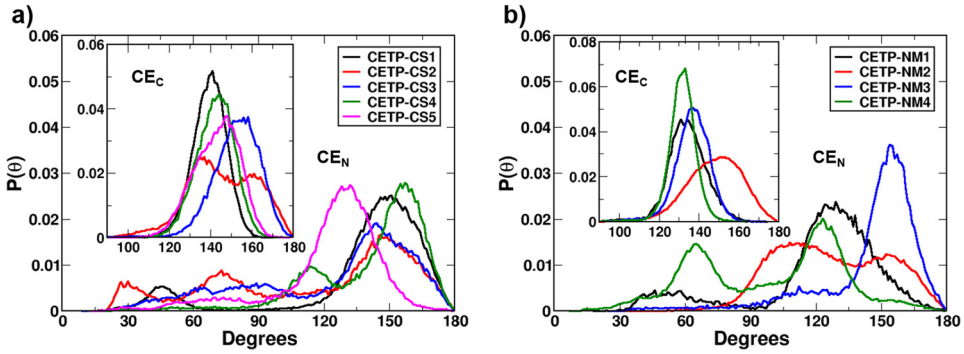

FIGURE 4. **Probability distribution of CE oleate angle.** Results are shown for CEs in CETP crystal structures (*a*) and CEs in NMA-derived CETP structures (*b*). Distribution is computed over the entire simulation time for each system.

high degrees of bending with the bending angle as high as 159° and bent to an arch-like conformation with a bending angle of 135°. In the same context, we estimated twisting-untwisting motion in CETP via relative rotation of N-terminal and C-terminal β-barrel domains with respect to the central β-domain. First, we constructed the axis of CETP as the vector connecting the COMs of N and C termini of the central β-domain and subsequently defined two planes, *P* and *Q*, with respect to the axis of CETP. Plane *P* is constituted by the axis of CETP and COM of the N-terminal β-barrel domain, whereas plane *Q* is constituted by the axis of CETP and COM of the C-terminal β-barrel domain. The twisting angle (θ_t) was computed by measuring the angle between the normal vectors $\hat{n}_1$ and $\hat{n}_2$ of these two planes as shown below.

$$\theta_t = \cos^{-1}(\hat{n}_1.\hat{n}_2/|\hat{n}_1||\hat{n}_2|) \quad \text{(Eq. 2)}$$

Fig. 5*b* shows the probability distribution of the twisting angle of CETP, pertaining to the twisting motions with respect to the crystal and normal mode conformations. The figure depicts a Gaussian distribution with an average torsional twist of ~8–12° in crystal structure simulations and a −2 to 16° twist in ANMA-generated CETP conformations. The average twisting angle observed in crystal conformations is less compared with the twisting observed in the normal modes, which can be attributed to the simplified harmonic description of the protein in ANMA.

The wide distribution of both bending and twisting angles indicates that CETP itself has enough plasticity and had undergone significant conformational changes in solution. To investigate whether these changes can influence the observed conformational switching of CE_N, we plotted the time evolution of the bending angle of CETP. As supplemental Fig. S3 shows, although there is no synergy between the motions of CE and CETP, CETP switches its conformation continuously. Moreover, the CETP conformation appeared to be more strained when CE_N was in the bent form. Thus, as supplemental Fig. S3 (*a* and *b*) indicates, the bending motion in CETP is more rapid, up to 300–500 ns, until when CE_N was undergoing a vigorous back-and-forth motion between the bent and linear conformation. After that time when CE_N became stabilized in the linear conformation, CETP bending also became less rapid. This was even more evident from the angle evolution of system CETP-CS4, where CETP bending was better stabilized at an earlier time of 250 ns in response to the early stability of CE_N to linear conformation (supplemental Fig. S3*c*). We further confirmed these findings of CETP influence on CE conformational switching by restraining the motion of CETP in a new test simulation (system 10 in supplemental Table S1). As supplemental Fig. S4 indicates, when CETP was restrained, the motions of CEs were completely restricted, with CE_N frozen into the original bent conformation. On the other hand, when CEs were kept fixed (system 11 in supplemental Table S1), CETP motion was found to be minimally hampered, as shown in supplemental Fig. S5. Thus, we conclude that CETP structure has sufficient plasticity, and the inherent dynamics of CETP greatly induces the conformational switching of its substrates, the cholesteryl esters.

CE Switching Enlarges CETP Core Tunnel—Because we observed a great deal of conformational flexibility of CEs within CETP, it was necessary to ascertain whether these frequent conformational changes in CEs affected the stability of secondary structural elements of CETP. Hence, we analyzed the evolution and stability of the whole secondary structural content and of local secondary structural elements of CETP around CE_N. We found that, although there were significant conformational changes in CEs in the core of CETP, the protein maintained a stable secondary structure throughout the simulation. The total number of residues that constitute different structural elements of the protein remained unchanged throughout the simulation time, suggesting no significant disruption of the CETP secondary elements (supplemental Fig. S6*a*). More specifically, the local secondary structural elements around CE_N, the central β-sheet (constituted by residues 11–16, 227–231, 261–266, and 456–461), helix A (residues 26–31), C-terminal region of helix B (residues 186–206), part of the N-terminal β-barrel twisted sheet (constituted by residues 81–86, 124–130, and 135–139), and the C-terminal region of helix B′ (residues 432–441) were completely stable during the entire course of a 1-μs simulation in the primary system (supplemental Fig. S6*b*). Analysis of secondary structure was performed by the GROMACS utility program do_dssp, which assigns secondary structure by analyzing the hydrogen bonding pattern between the protein residues.

As mentioned previously, the substrate-bound CETP crystal structure was seen to possess a hydrophobic tunnel of length 60 Å and volume 2560 $Å^3$ occupied by the two CEs and two dio-

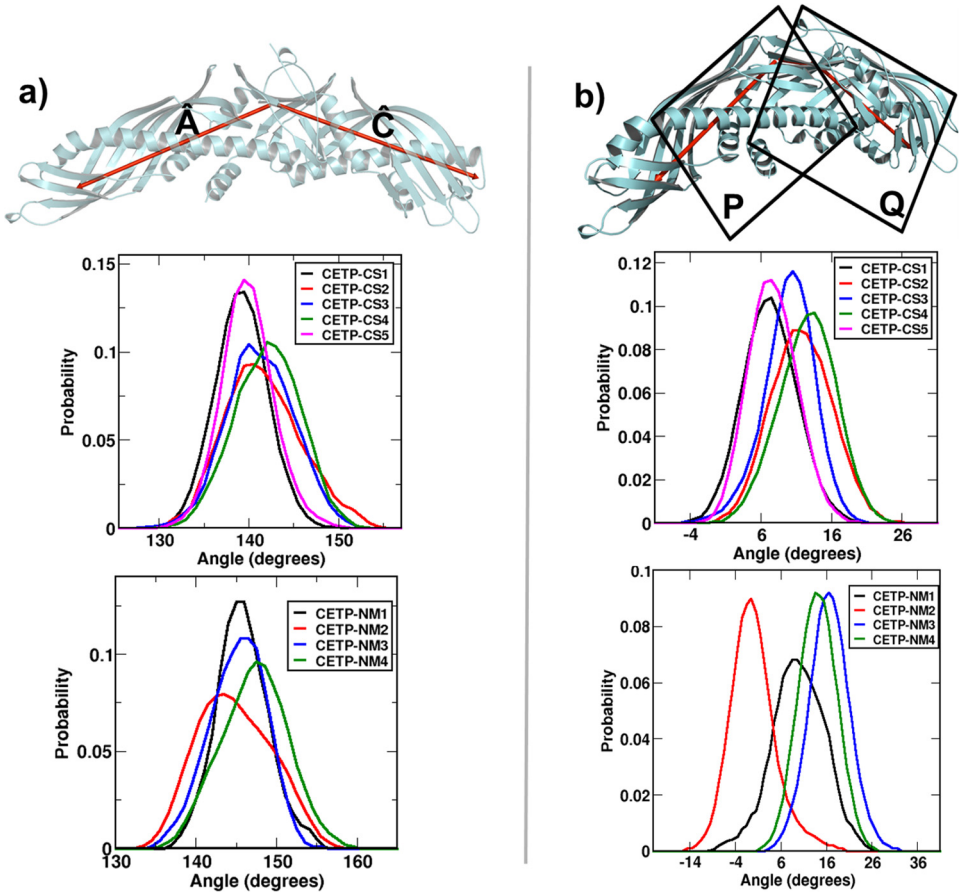

FIGURE 5. **Quantification of bending and twisting motions in CETP.** *a*, probability distribution of CETP bending angle. Bending was computed from the angle between two vectors, $\hat{A}$ and $\hat{C}$, as shown in *red* on the molecular frame of CETP. *b*, probability distribution of the CETP twist angle. Twisting was computed by measuring the angle between the two planes, *P* and *Q*, as shown.

leoylphosphatidylcholine molecules (23). The observed conformational flexibility of CEs and the inherent plasticity of CETP have impelled us to examine the plausible changes in the CETP hydrophobic tunnel. Hence, we examined the evolution of the CETP core tunnel across the 1-μs simulation run in the primary CETP system. Very interestingly, as Fig. 6 shows, the CETP tunnel significantly elongates from the crystal conformation and stabilized to an extended length of ~95 Å during the final 500-ns simulation time when CE_N was linear. This finding is consistent with the recent EM structure of CETP bound to HDL and LDL, which suggested a more continuous hydrophobic tunnel, compared with the shorter 60-Å central cavity observed in the CETP crystal structure (21). We speculate that the constricted tunnel found in the CETP crystal structure is a consequence of the crystal packing effects, as was also observed in the crystal structures of other proteins (*e.g.* HIV-1 protease) (31). Thus, it appears that the otherwise flexible CE was trapped in a bent conformation in the crystal that corresponds to a strongly packed complex of CE_N and CETP (further discussed below). In our simulations, as the CETP-CE complex was provided a higher temperature (310 K *versus* 100 K in crystal) and also the solution phase, the system relaxed to an energetically more favorable conformation, with CE_N turning to linear. The computed energy difference between the average structure of linear CE-bound CETP and the crystal conformation is −6.53 kcal/mol (ΔE_{linear_CE} = −85.74 ± 1.2 kcal/mol; $\Delta E_{crystal}$ = −79.21 kcal/mol). The small difference in energetics is again suggestive of their coexistence in solution.

To have a clearer visualization of the CETP core tunnel, we extracted all CETP conformations with tunnel length ≥95 Å from the final 500-ns simulation data. The average conformation of CETP from this ensemble of structures is presented in Fig. 7*a*. The continuous tunnel traversing from the N- to C-terminal end of CETP is evident from this figure. In contrast, the 60-Å tunnel in the crystal conformation is confined at the central domain of the protein (Fig. 7*b*). We have also quantified the radius across the tunnel length and computed the total tunnel volume. The existence of a finite radius across the tunnel confirms that the protein indeed creates a continuous tunnel traversing from the N- to C-terminal end (Fig. 7*c*). The tunnel volume of the ensemble-averaged structure was 3536 $Å^3$, and the radius was 1.4–2.1 Å wider than the crystal conformation. For comparison, we have also done the same analysis on the simulation trajectory of the CETP-NM4 system, and the results are included in Fig. 7*c*. A more elongated and continuous tunnel traversing up to the C-terminal edge is consistent with the more relaxed nature of this conformation of CETP. In parallel, to check the effect of CE linearization on tunnel length, we measured the CETP tunnel in a new simulation system (system 12 in supplemental Table S1), where CE_N was restrained in the bent conformation. As supplemental Fig. S7 shows, the CETP tunnel remained constricted to 65 Å, suggesting that the conforma-

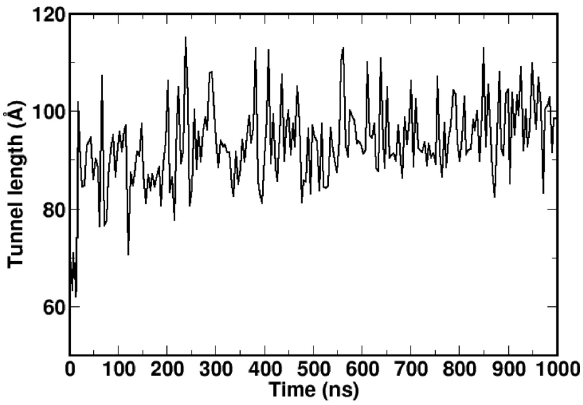

FIGURE 6. **Time evolution of the CETP core tunnel along the 1-μs simulation run in the primary system (system 1).** The CETP tunnel significantly elongated from the crystal conformation and stabilized to an extended length of ~95 Å during the final 500 ns of simulation time when CE_N became linear.

tional switching of CE greatly assists the formation of a continuous tunnel across CETP. Taken together, it appears that the inherent plasticity in CETP structure and the induced linearization of bound CEs produce a long continuous tunnel spanning from the N- to C-terminal ends of CETP, which could facilitate the transfer of lipids between lipoproteins. The associated large scale conformational changes in CETP and CE can happen in solution phase and, more prominently, when CETP encounters the lipoproteins, an environment that we attempted to create here by performing normal mode analysis on CETP.

Linear CE Loses Contacts with CETP but Gains New Contacts with a Second CE—To underscore the possible reason why CE_N was trapped in the bent conformation in crystal, we analyzed the interactions of bent CE_N with CETP tunnel lining residues and compared that with the interactions of linear CE_N. The results are shown in Fig. 8. Unsurprisingly, both bent and linear CE_N conformations have many common hydrophobic interactions with CETP residues (*e.g.* Ile-11 and Cys-13 in strand S1; Val-30 and Ile-31 in helix A; Ile-82 and Val-84 in strand S4; Ile-125 and Leu-129 in strand S5; Val-136 and Thr-138 in strand S6; Ile-187, Ser-191, Ala-195, Val-198, Gln-199, Ala-202, and Leu-206 in helix B; Ile-215 in strand S7; His-232 in strand S8; Phe-263 and Phe-265 in strand S1′; Met-433 and Val-438 in helix B′; Leu-457 in strand S8′). Apart from the CETP residues, CE_C and N-terminal phospholipid also maintained similar interactions with both forms of CE_N. However, CE_N in the linear conformation had lost interactions with other tunnel residues of CETP (*e.g.* Ile-15 in strand S1; Leu-23 and Thr-27 in helix A; Ile-86 in strand S4; Thr-127 in strand S5; Ile-205 in helix B; Leu-228 and Ser-230 in strand S8; Leu-261 in strand S1′; Phe-441 and Ile-443 in strand S7′; Met-459 and Phe-461 in strand S8′) but gained new hydrophobic contacts with residues Ala-34 in helix A; Met-194 in helix B; Leu-217 in strand S7; Phe-270 in helix A′; Lys-436 in helix B′; Phe-471 and Leu-472 in helix X; and the C-terminal phospholipid, PL-2 (Fig. 8, compare *a* and *b*). Thus, there was a net loss of five residue-level contacts due to the linearization of bent CE_N, which made 36 residue-level contacts in the crystal, accounting for a net loss of 14% residue-level contacts of linear CE relative to the bent form. In terms of site-site contacts, this loss appears to be even more prominent. A net loss of 20 distinct site-site contacts was observed due to the conformational transition of bent CE to the linear form (Fig. 8*c*). Site-site contacts were counted by imposing a distance criterion of 5 Å between a pair of protein and CE_N atoms. These findings strengthen our inference of crystal packing effects in the solved crystal structure, because the CE_N experiences a greater packing (larger contacts) with CETP residues in the bent form. In our simulations, as the CETP-CE complex was provided a higher temperature (310 K *versus* 100 K in crystal) and also the solution phase, the system relaxed to a thermodynamically more favorable conformation, with CE_N turning to linear.

The other noteworthy feature of Fig. 8*c* is that despite the significant changes in CE_N, CE_C maintained very similar contacts with CETP tunnel residues throughout the simulation. More importantly, the oleate chain of CE_N tended to form a new set of hydrophobic contacts with the acyl chain of CE_C to compensate for its loss of contacts with CETP tunnel residues. Thus, the initial number of 2–10 site-site contacts of CE_N with CE_C was increased to 10–20 due to the extended linear CE_N conformation. From these results, we are tempted to speculate that the reduced contacts of linear CE_N with CETP and its increased contacts with CE_C reduce the friction of CEs with the CETP tunnel and facilitate the transfer of these neutral lipids through a continuous CETP tunnel. Thus, our MD simulation result could successfully produce the "open state" of CETP, as was speculated by Ren and co-workers (21) from their recent cryo-EM study on the lipid transfer mechanism of CETP.

Straightening of CE Is Boosted by Free Energy Gain—Thus far, we have seen that CETP-bound CE switches conformation from bent to linear, and this process is assisted by the inherent dynamics of CETP and favorable contacts of its tunnel residues. To assess the energetic contribution of individual CETP residues on conformational switching of CE_N, we performed a Gibbs free energy calculation and decomposed the total Gibbs energy into residue level. A set of 10,000 frames between 200 and 300 ns, when CE_N was in the bent conformation, and another set of 10,000 frames between 600 and 700 ns, when CE_N was in linear conformation, were analyzed. Subsequently, free energy gain due to CE conformational change from bent to linear ($\Delta\Delta G_{\text{linear-bent}}$) was calculated for each CETP residue, and the results are presented in Fig. 9. Free energy contributions are shown only for those CETP residues that pass the free energy difference cut-off of $\pm$0.5 kcal/mol.

As Fig. 9 shows, bent CE_N has stronger binding affinity for the central β domain residues (Arg-14, Met-260, Leu-261, Phe-441, and Phe-461) and the N-terminal phospholipid, PL_N. On the other hand, CE_N in the linear conformation has greater binding strength with the central β domain residues Ile-11, Phe-265, and Phe-270; helix B′ residue Met-433; helix B residue Ile-205; strand S7 residue Gly-212; strand S8 residue His-235; C-terminal residue Ser-476; and the lipids present in the C-terminal hydrophobic pocket, CE_C and PL_C. This free energy result fits very well with contact analysis data, because most of the strongly interacting CETP residues (*e.g.* Ile-11, Ile-205, Leu-261, Phe-265, Phe-270, Met-433, Phe-441, and Phe-461) were also found to make contacts with bent or/and linear CE_N (compare Figs. 8 and 9). As mentioned above, residues Ile-11, Phe-

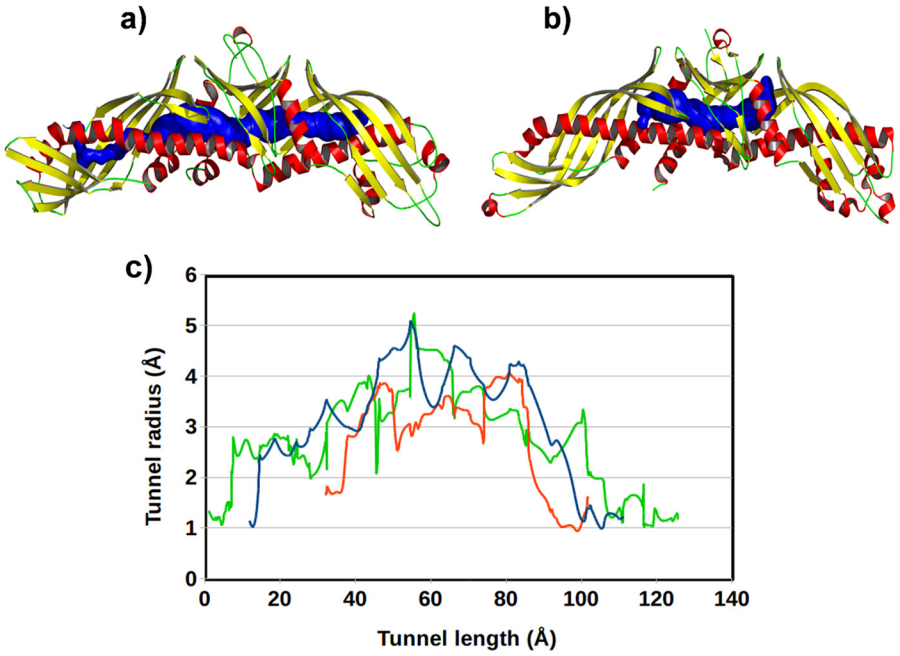

FIGURE 7. **Elongation of the CETP core tunnel during simulations.** *a*, tunnel in the extended CETP structure; *b*, tunnel in the crystal structure. CETP is shown in a *schematic representation*, and the tunnel is shown in *blue surface mode*. *c*, CETP tunnel radius as a function of tunnel length. Results are shown for CETP in crystal structure (*red*), CETP in extended conformation from crystal structure simulation (*blue*), and CETP in extended conformation from simulation of NMA-derived CETP structure (*green*). Simulation structures are ensemble-averaged over at least 1000 extended conformations of CETP.

265, and Met-433 make contacts with both forms of CE_N. However, the free energy of binding of these residues with linear CE_N is much stronger than with the bent form. Moreover, Phe-270, Gly-212, His-235, Ser-476, etc. engage in specific interactions with linear CE_N that are energetically highly favorable. Although the interactions of Arg-14, Met-260, Leu-261, Phe-441, and Phe-461 tend to favor the bent form of CE_N, there is a net gain of −5.55 kcal/mol (−85.74 ± 1.2 kcal/mol for linear CE *versus* −80.19 ± 1.3 kcal/mol for bent CE) for linear CE in the CETP tunnel when in solution.

Interestingly, a subset of our identified residues with significant affinity for linear CE_N has recently been reported to be crucial for CE/TG transfer through CETP and CETP stability (23). For example, the mutant M433W exhibited a nearly 2-fold decline in CE transfer activity and a 5-fold decline in TG transfer activity in the site-specific mutagenesis studies (23). Similarly, the mutants F265R and F270R were characterized to be responsible for misfolding and subsequent failure in CETP secretion (23). The deletion of Ser-476 from CETP C-terminal had completely abolished the protein's neutral lipid transfer activity (32). In other words, these reports have pointed out that residues Met-433, Phe-265, Phe-270, and Ser-476 in native CETP maintain the structural integrity and functional activity of the protein. Now, because the functional activity of CETP is the transfer of CE/TG and none of the mutational studies have traced any of our identified CETP residues interacting with the bent form of CE for activity (Fig. 9), it is conceivable that CE remains in the linear conformation in functional CETP, whereas the specific CETP residues (*e.g.* the *green-colored* residues in Fig. 9) provide a favorable environment.

Conclusions—Understanding the mechanism of lipid transfer by CETP has received tremendous attention due to its crucial role in maintaining the levels of HDL and LDL. Although the CE-bound CETP crystal structure provided much useful structural information, understanding a dynamic process, such as the transfer of lipids through CETP, remains elusive. In this study, we employed microsecond-long atomistic MD simulations and normal mode analysis to explore the dynamics of CETP and its bound substrates, which provided very important clues about the lipid transfer activity of CETP. Our results suggested unique structural plasticity in the CETP structure, consisting of bending-unbending and twisting motions along its long axis. This inherent dynamics of CETP greatly induces the conformational switching of CEs, which transform to a linear conformation from their bent structure in crystal. We speculate that the bent CE and constricted tunnel found in the CETP crystal structure are the consequence of crystal packing effects, as was also observed in the crystal structures of other proteins (*e.g.* HIV-1 protease) (31). In our simulations, as the CETP-CE complex was provided a higher temperature (310 K *versus* 100 K in crystal) and also the solution phase, the system relaxed to a thermodynamically stable conformation, with bound CEs switching to linear. As a consequence of the inherent plasticity of CETP and the induced linearization of bound CEs, a long continuous tunnel spanning from N- to C-terminal ends of CETP is produced, which can facilitate the transfer of lipids between lipoproteins. Thus, our MD simulation results could successfully produce the "open state" of CETP, as was speculated by Ren and co-workers (21) from their recent EM study on the lipid transfer mechanism of CETP.

When this work was in progress, Ren and co-workers (25) reported the transfer pathway of CE through CETP by MD simulation studies. To detect the pathway in a reasonable time, the authors applied an external force to pull a linear CE molecule through a hollow CETP tunnel. Very similar to this study, our results also show the twisting motions in CETP and the

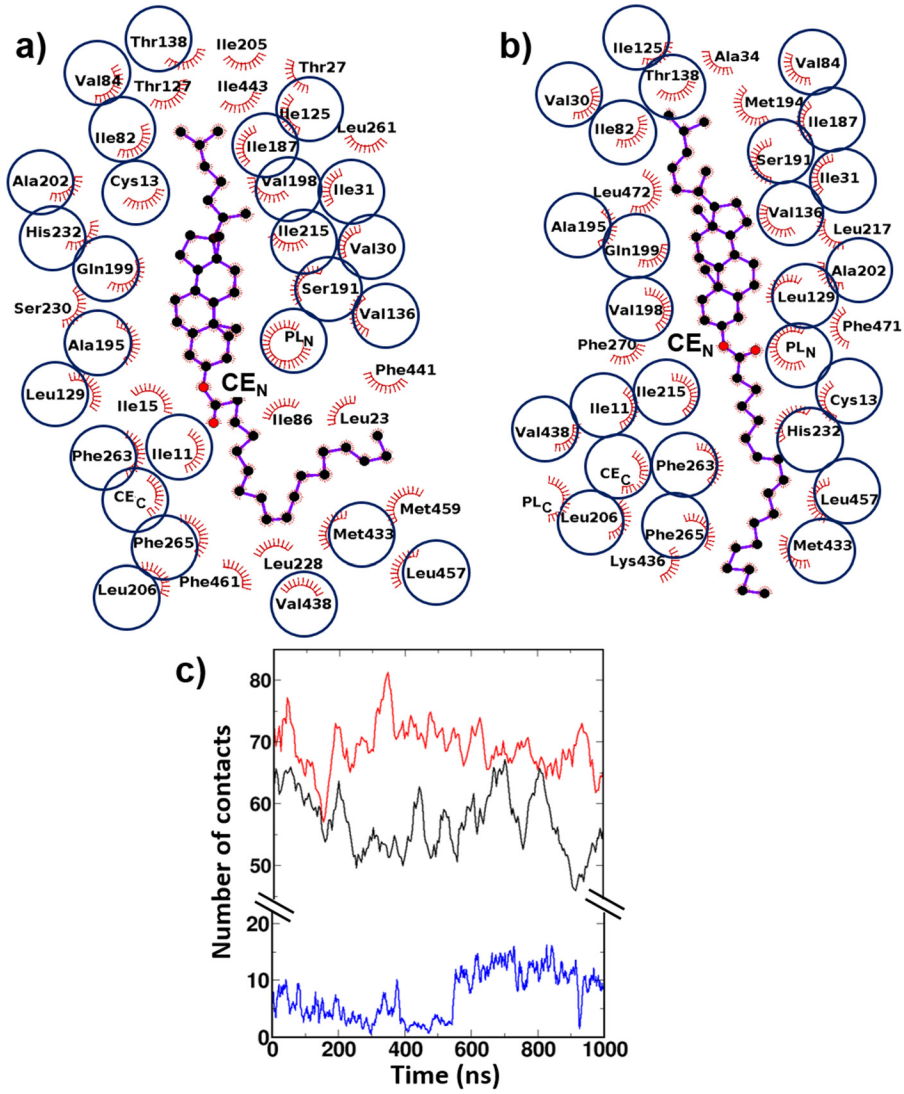

FIGURE 8. **Hydrophobic contacts of different conformation of CEs with CETP.** Results are shown for bent CE conformation (*a*) and linear CE conformation (*b*). CEs are shown by a *ball-and-stick representation*, and the protein residues involved in hydrophobic interactions are shown by *red spikes*. The common interacting CETP residues are highlighted by *circles*. *c*, time evolution of the site-site contacts between CE_N and CE_C (*blue*), CE_N and CETP (*black*), and CE_C and CETP (*red*).

formation of a continuous tunnel between the two distal ends of CETP. Moreover, the CETP tunnel lining residues that we found to make favorable interactions with CE (*e.g.* residues Ile-205, Phe-263, Phe-265, and Met-433) were noted by these authors to facilitate the CE transfer. However, the tunnel length from our CETP crystal structure simulation was found to be shorter by about 15 Å than that in the report by Ren and co-workers (95 Å *versus* 110 Å), which explicitly included the lipoprotein mimics at both ends of CETP to model the HDL-CETP-LDL ternary complex. Our implicit inclusion of lipoprotein effects by simulating the relaxed CETP generated from NMA, however, produced a continuous core tunnel as lengthy as the aforementioned report. In addition, our study's major focus on the inherent dynamics of CETP shows that, apart from the twisting motion, CETP also undergoes significant bending-unbending that could produce sufficient driving force "within" to induce conformational switching in bound CE and consequently a continuous tunnel across CETP. Although this tunnel could become more prominent when CETP senses the lipoproteins, it can exist in the free form of the protein due to its structural plasticity in solution.

Materials and Methods

A molecular dynamics simulation of the primary CETP system was started from the recently solved x-ray crystal structure of CETP (Protein Data Bank entry 2OBD). The missing residues in the N-terminal region of the crystal structure (Ala-1, Ser-2, Lys-3, and Gly-4) were included using MODELLER9 version 13 (33). Subsequently, the mutations induced in CETP to promote the crystallization (*viz.* C1A, N88D, C131A, N240D, and N341D) were back-mutated. The charge state of CETP was chosen at pH 7.4 to mimic the physiological conditions. The GROMOS53A6 force field (34) for the protein and Berger lipid parameters (35) for CETP bound lipids were used. Hydrogens for heavy atoms were added by the pdb2gmx module in the GROMACS-4.5.5 simulation package. The protonation states of histidines were determined by the local hydrogen bonding network using the WHAT IF web server (36). The system was

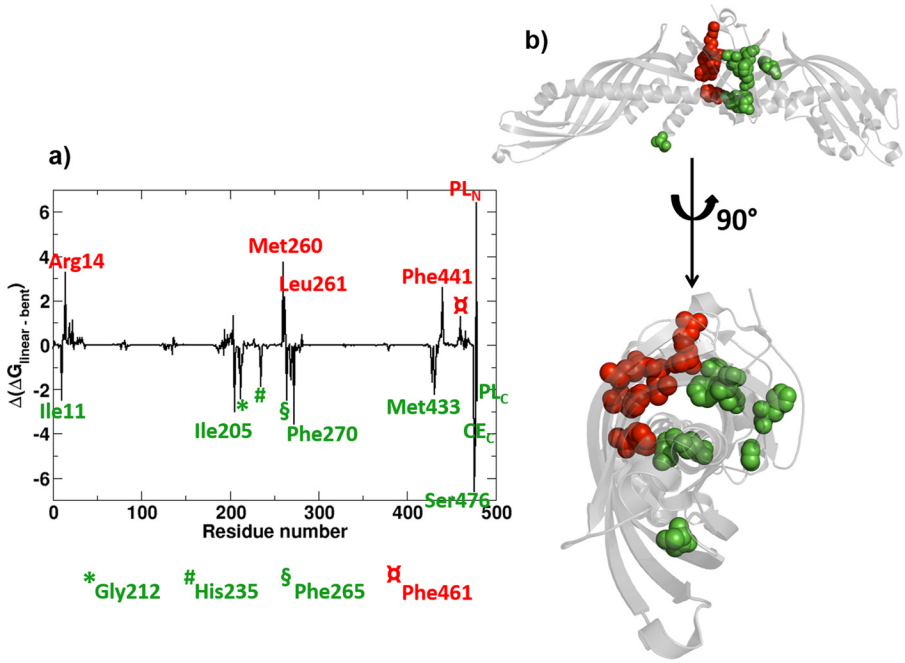

FIGURE 9. *a*, change in Gibbs free energy of select CETP residues due to the conformational transition of CE_N from bent to linear. Residues favoring the CE_N linearization are highlighted in *green*, and those favor bent CE_N are highlighted in *red*. *b*, location of these CETP tunnel lining residues are shown in the three-dimensional representation of the protein.

subsequently energy-minimized for 2000 steps using the conjugate gradient algorithm and another 2000 steps using the steepest descent algorithm. The structure was solvated using explicit water in a cubic periodic box with water molecules extending 10 Å outside the protein on all sides. Water molecules were described using a simple point charge water model. The system was solvated using 131,251 water molecules, and a salt concentration of 0.15 M was maintained by adding 371 Na^+ and 363 Cl^- counterions. The system was energy-minimized again and then heated up gradually to reach a temperature of 310 K using a V-rescale thermostat with a coupling constant of 0.1 ps (37). The solvent density was adjusted under isobaric and isothermal conditions at 1 bar and 310 K. A Parrinello-Rahman barostat with isotropic pressure coupling and a coupling constant of 0.1 ps was used to set the pressure at 1 bar (38). The system was equilibrated for 10 ns in the NPT ensemble with a simulation time step of 2 fs. Finally, the production run was carried out for 1000 ns in the NPT ensemble for the primary system (system CETP-CS1 in supplemental Table S1). The long range electrostatic interactions were treated using particle-mesh Ewald sum with a cut-off of 1.0 nm (39). The van der Waals interactions were terminated beyond the cut-off value of 1.0 nm. The LINCS algorithm was used to constrain all bonds involving hydrogen atoms (40). All simulations were performed using the GROMACS-4.5.5 simulation program (41).

The molecular dynamics simulations of CETP crystal structure essentially describe the conformational changes in CETP that occur at short length and time scales. However, the changes that CETP undergoes in plasma and particularly when bound to lipoprotein would be at much larger scales. To capture such large scale conformational changes, we performed NMA on the CETP structure obtained from crystal. NMA is a well tested technique that identifies slow, large amplitude motions by investigating the low frequency vibrational modes of a protein described by an elastic network (30). The anisotropic network model web server, ANM 2.0, was used to perform the NMA (42, 43). In the elastic model of CETP, the maximum interaction range between the C_α atoms (nodes) was set at 15 Å. First the four lowest frequency vibrational modes were picked from NMA, which presumably represent the most relaxed/functionally relevant conformations of CETP as it exists in plasma or when bound to lipoproteins. These four relaxed or functionally relevant CETP conformations were designated CETP-NM1, CETP-NM2, CETP-NM3, and CETP-NM4. Subsequently, to explore the dynamics, the four lipids (two CEs and two PLs) were docked at the requisite locations of the CETP tunnel, and the complex was subjected to long molecular dynamics simulations following the same protocol as described for the primary system. Supplemental Table S1 lists all of the systems studied. Overall, a total of 5.9 μs of atomistic simulation was carried out in this work.

The Caver version 3.0 tool kit was used to identify and characterize the pockets and tunnels in CETP (44). Various conformations of CETP after removing the lipids were given as inputs for tunnel analysis. The probe radius was set to the default of 3 Å to construct the molecular surface of the pocket or tunnel. PyMOL was used to generate all structural figures (45). The LIGPLOT tool was used to map all protein-lipid interactions (46).

Free Energy Calculations—The free energy calculations were performed on the molecular dynamics trajectories using the molecular mechanics Poisson Boltzmann surface area method (47). The GROMACS utility program g_mmpbsa was employed to estimate the free energies (48). Generally, the binding free energy for a ligand bound protein in solvent is estimated as follows,

$$\Delta G_{binding} = G_{complex} - (G_{protein} + G_{ligand}) \quad \text{(Eq. 3)}$$

where $G_{complex}$, $G_{protein}$, and G_{ligand} are the free energies of the protein-ligand complex, free protein, and free ligand, respectively, in solvent.

The average free energy for each individual component in the above equation is defined as follows,

$$G_i = \langle G_S \rangle + \langle E_{MM} \rangle - TS \quad \text{(Eq. 4)}$$

where TS is the contribution of entropy to the system's free energy at temperature T in vacuum, and $\langle E_{MM} \rangle$ is the vacuum potential energy, which includes bonded and non-bonded interaction energies and can be expressed as follows.

$$E_{MM} = E_{bonded} + E_{nonbonded} \quad \text{(Eq. 5)}$$

$\langle G_S \rangle$ is the solvation free energy and is expressed as follows,

$$G_S = G_{nonpolar} + G_{polar} \quad \text{(Eq. 6)}$$

where $G_{nonpolar}$ and G_{polar} represent the contribution of nonpolar and polar solvation energy.

Subsequently, the binding energy for each individual residue (ΔG_r) was decomposed as follows,

$$\Delta G_r = \sum_{j=0}^{n} (G_j^{complex} - G_j^{free}) \quad \text{(Eq. 7)}$$

where $G_j^{complex}$ and G_j^{free} are the energies of the jth atom from the r residue in complex and free forms, respectively, and n is the total number of atoms in the residue. The vacuum, solute, and solvent dielectric constants were set at 1, 2, and 80, respectively. Bootstrap analysis was performed to obtain S.E. values.

Author Contributions—V. R. C., P. D. R., and S. S. conceived and designed the experiments. V. R. C. and P. D. R. performed the experiments. V. R. C., P. D. R., and S. S. analyzed the data. S. S. contributed reagents, materials, and analysis tools. V. R. C., P. D. R., and S. S. wrote the paper.

Acknowledgment—We thank the High Performance Computing Environment (HPCE), Indian Institute of Technology Madras, for computational resources.

References

1. Sharrett, A. R., Ballantyne, C. M., Coady, S. A., Heiss, G., Sorlie, P. D., Catellier, D., Patsch, W., and Atherosclerosis Risk in Communities Study Group (2001) Coronary heart disease prediction from lipoprotein cholesterol levels, triglycerides, lipoprotein(a), apolipoproteins A-I and B, and HDL density subfractions: the atherosclerosis risk in communities (ARIC) study. *Circulation* **104,** 1108–1113
2. Luc, G., Bard, J.-M., Ferrières, J., Evans, A., Amouyel, P., Arveiler, D., Fruchart, J. C., and Ducimetière, P. (2002) Value of HDL cholesterol, apolipoprotein A-I, lipoprotein A-I, and lipoprotein A-I/A-II in prediction of coronary heart disease: The PRIME study. *Arterioscler. Thromb. Vasc. Biol.* **22,** 1155–1161
3. Zhang, Y., Zanotti, I., Reilly, M. P., Glick, J. M., Rothblat, G. H., and Rader, D. J. (2003) Overexpression of apolipoprotein A-I promotes reverse transport of cholesterol from macrophages to feces *in vivo*. *Circulation* **108,** 661–663
4. Tall, A. R., Yvan-Charvet, L., Terasaka, N., Pagler, T., and Wang, N. (2008) HDL, ABC transporters, and cholesterol efflux: implications for the treatment of atherosclerosis. *Cell Metab.* **7,** 365–375
5. Cannon, C. P., Braunwald, E., McCabe, C. H., Rader, D. J., Rouleau, J. L., Belder, R., Joyal, S. V., Hill, K. A., Pfeffer, M. A., Skene, A. M., and Pravastatin or Atorvastatin Evaluation and Infection Therapy-Thrombolysis in Myocardial Infarction 22 Investigators (2004) Intensive versus moderate lipid lowering with statins after acute coronary syndromes. *N. Engl. J. Med.* **350,** 1495–1504
6. Robins, S. J., Collins, D., Wittes, J. T., Papademetriou, V., Deedwania, P. C., Schaefer, E. J., McNamara, J. R., Kashyap, M. L., Hershman, J. M., Wexler, L. F., Rubins, H. B., and VA-HIT Study Group. Veterans Affairs High-Density Lipoprotein Intervention Trial (2001) Relation of gemfibrozil treatment and lipid levels with major coronary events: VA-HIT: a randomized controlled trial. *JAMA* **285,** 1585–1591
7. Goldberg, A., Alagona, P., Jr., Capuzzi, D. M., Guyton, J., Morgan, J. M., Rodgers, J., Sachson, R., and Samuel, P. (2000) Multiple-dose efficacy and safety of an extended-release form of niacin in the management of hyperlipidemia. *Am. J. Cardiol.* **85,** 1100–1105
8. Tall, A. R. (1993) Plasma cholesteryl ester transfer protein. *J. Lipid Res.* **34,** 1255–1274
9. Barter, P. J., Brewer, H. B., Jr., Chapman, M. J., Hennekens, C. H., Rader, D. J., and Tall, A. R. (2003) Cholesteryl ester transfer protein: A novel target for raising HDL and inhibiting atherosclerosis. *Arterioscler. Thromb. Vasc. Biol.* **23,** 160–167
10. Zhong, S., Sharp, D. S., Grove, J. S., Bruce, C., Yano, K., Curb, J. D., and Tall, A. R. (1996) Increased coronary heart disease in Japanese-American men with mutation in the cholesteryl ester transfer protein gene despite increased HDL levels. *J. Clin. Invest.* **97,** 2917–2923
11. Koizumi, J., Mabuchi, H., Yoshimura, A., Michishita, I., Takeda, M., Itoh, H., Sakai, Y., Sakai, T., Ueda, K., and Takeda, R. (1985) Deficiency of serum cholesteryl-ester transfer activity in patients with familial hyperalphalipoproteinaemia. *Atherosclerosis* **58,** 175–186
12. Brown, M. L., Inazu, A., Hesler, C. B., Agellon, L. B., Mann, C., Whitlock, M. E., Marcel, Y. L., Milne, R. W., Koizumi, J., and Mabuchi, H. (1989) Molecular basis of lipid transfer protein deficiency in a family with increased high-density lipoproteins. *Nature* **342,** 448–451
13. Inazu, A., Brown, M. L., Hesler, C. B., Agellon, L. B., Koizumi, J., Takata, K., Maruhama, Y., Mabuchi, H., and Tall, A. R. (1990) Increased high-density lipoprotein levels caused by a common cholesteryl-ester transfer protein gene mutation. *N. Engl. J. Med.* **323,** 1234–1238
14. Marotti, K. R., Castle, C. K., Boyle, T. P., Lin, A. H., Murray, R. W., and Melchior, G. W. (1993) Severe atherosclerosis in transgenic mice expressing simian cholesteryl ester transfer protein. *Nature* **364,** 73–75
15. Plump, A. S., Masucci-Magoulas, L., Bruce, C., Bisgaier, C. L., Breslow, J. L., and Tall, A. R. (1999) Increased atherosclerosis in ApoE and LDL receptor gene knock-out mice as a result of human cholesteryl ester transfer protein transgene expression. *Arterioscler. Thromb. Vasc. Biol.* **19,** 1105–1110
16. Sugano, M., Makino, N., Sawada, S., Otsuka, S., Watanabe, M., Okamoto, H., Kamada, M., and Mizushima, A. (1998) Effect of antisense oligonucleotides against cholesteryl ester transfer protein on the development of atherosclerosis in cholesterol-fed rabbits. *J. Biol. Chem.* **273,** 5033–5036
17. Mantlo, N. B., and Escribano, A. (2014) Update on the discovery and development of cholesteryl ester transfer protein inhibitors for reducing residual cardiovascular risk. *J. Med. Chem.* **57,** 1–17
18. Sikorski, J. A. (2006) Oral cholesteryl ester transfer protein (CETP) inhibitors: a potential new approach for treating coronary artery disease. *J. Med. Chem.* **49,** 1–22
19. Gotto, A. M., Jr., and Moon, J. E. (2012) Safety of inhibition of cholesteryl ester transfer protein with anacetrapib: the DEFINE study. *Expert Rev. Cardiovasc. Ther.* **10,** 955–963
20. Nicholls, S. J., Brewer, H. B., Kastelein, J. J. P., Krueger, K. A., Wang, M. D., Shao, M., Hu, B., McErlean, E., and Nissen, S. E. (2011) Effects of the CETP inhibitor evacetrapib administered as monotherapy or in combination with statins on HDL and LDL cholesterol: a randomized controlled trial. *JAMA* **306,** 2099–2109
21. Zhang, L., Yan, F., Zhang, S., Lei, D., Charles, M. A., Cavigiolio, G., Oda, M., Krauss, R. M., Weisgraber, K. H., Rye K.-A., Pownall, H. J., Qiu, X., and Ren, G. (2012) Structural basis of transfer between lipoproteins by cholesteryl ester transfer protein. *Nat. Chem. Biol.* **8,** 342–349

22. Lauer, M. E., Graff-Meyer, A., Rufer, A. C., Maugeais, C., von der Mark, E., Matile, H., D'Arcy, B., Magg, C., Ringler, P., Müller, S. A., Scherer, S., Dernick, G., Thoma, R., Hennig, M., Niesor, E. J., and Stahlberg, H. (2016) Cholesteryl ester transfer between lipoproteins does not require a ternary tunnel complex with CETP. *J. Struct. Biol.* **194,** 191–198
23. Qiu, X., Mistry, A., Ammirati, M. J., Chrunyk, B. A., Clark, R. W., Cong, Y., Culp, J. S., Danley, D. E., Freeman, T. B., Geoghegan, K. F., Griffor, M. C., Hawrylik, S. J., Hayward, C. M., Hensley, P., Hoth, L. R., *et al.* (2007) Crystal structure of cholesteryl ester transfer protein reveals a long tunnel and four bound lipid molecules. *Nat. Struct. Mol. Biol.* **14,** 106–113
24. Liu, S., Mistry, A., Reynolds, J. M., Lloyd, D. B., Griffor, M. C., Perry, D. A., Ruggeri, R. B., Clark, R. W., and Qiu, X. (2012) Crystal structures of cholesteryl ester transfer protein in complex with inhibitors. *J. Biol. Chem.* **287,** 37321–37329
25. Lei, D., Rames, M., Zhang, X., Zhang, L., Zhang, S., and Ren, G. (2016) Insights into the tunnel mechanism of cholesteryl ester transfer protein using all-atom molecular dynamics simulations. *J. Biol. Chem.* **291,** 14034–14044
26. Chirasani, V. R., Sankar, R., and Senapati, S. (2016) Mechanism of inhibition of cholesteryl ester transfer protein by small molecule inhibitors. *J. Phys. Chem. B.* 10.1021/acs.jpcb.6b01928
27. Koivuniemi, A., Vuorela, T., Kovanen, P. T., Vattulainen, I., and Hyvönen, M. T. (2012) Lipid exchange mechanism of the cholesteryl ester transfer protein clarified by atomistic and coarse-grained simulations. *PLoS Comput. Biol.* **8,** e1002299
28. Äijänen, T., Koivuniemi A., Javanainen, M., Rissanen, S., Rog, T., and Vattulainen, I. (2014) How anacetrapib inhibits the activity of the cholesteryl ester transfer protein? Perspective through atomistic simulations. *PLoS Comput. Biol.* **10,** e1003987
29. Senapati, S., and Berkowitz, M. L. (2003) Molecular dynamics simulation studies of polyether and perfluoropolyether surfactant based reverse micelles in supercritical carbon dioxide. *J. Phys. Chem. B* **107,** 12906–12916
30. Alexandrov, V., Lehnert, U., Echols, N., Milburn, D., Engelman, D., and Gerstein, M. (2005) Normal modes for predicting protein motions: a comprehensive database assessment and associated Web tool. *Protein Sci.* **14,** 633–643
31. Layten, M., Hornak, V., and Simmerling, C. (2006) The open structure of a multi-drug-resistant HIV-1 protease is stabilized by crystal packing contacts. *J. Am. Chem. Soc.* **128,** 13360–13361
32. Wang, S., Kussie, P., Deng, L., and Tall, A. (1995) Defective binding of neutral lipids by a carboxyl-terminal deletion mutant of cholesteryl ester transfer protein: evidence for a carboxyl-terminal cholesteryl ester binding site essential for neutral lipid transfer activity. *J. Biol. Chem.* **270,** 612–618
33. Webb, B., and Sali, A. (2014) Comparative protein structure modeling using Modeller. *Curr. Protoc. Bioinformatics* **47,** 5.6.1–5.6.37
34. Schuler, L. D., Daura, X., and van Gunsteren, W. F. (2001) An improved GROMOS96 force field for aliphatic hydrocarbons in the condensed phase. *J. Comput. Chem.* **22,** 1205–1218
35. Berger, O., Edholm, O., and Jähnig, F. (1997) Molecular dynamics simulations of a fluid bilayer of dipalmitoylphosphatidylcholine at full hydration, constant pressure, and constant temperature. *Biophys. J.* **72,** 2002–2013
36. Vriend, G. (1990) WHAT IF: a molecular modeling and drug design program. *J. Mol. Graph.* **8,** 52–56, 29.
37. Bussi, G., Donadio, D., and Parrinello, M. (2007) Canonical sampling through velocity rescaling. *J. Chem. Phys.* **126,** 014101
38. Parrinello, M., and Rahman, A. (1981) Polymorphic transitions in single crystals: a new molecular dynamics method. *J. Appl. Phys.* **52,** 7182–7190
39. Essmann, U., Perera, L., Berkowitz, M. L., Darden, T., Lee, H., and Pedersen, L. G. (1995) A smooth particle mesh Ewald method. *J. Chem. Phys.* **103,** 8577–8593
40. Hess, B., Bekker, H., Berendsen, H. J. C., and Fraaije, J. G. E. M. (1997) LINCS: a linear constraint solver for molecular simulations. *J. Comput. Chem.* **18,** 1463–1472
41. Hess, B., Kutzner, C., van der Spoel, D., and Lindahl, E. (2008) GROMACS 4: algorithms for highly efficient, load-balanced, and scalable molecular simulation. *J. Chem. Theory Comput.* **4,** 435–447
42. Eyal, E., Yang, L. W., and Bahar, I. (2006) Anisotropic network model : systematic evaluation and a new web interface. *Bioinformatics* **22,** 2619–2627
43. Doruker, P., Atilgan, A. R., and Bahar, I. (2000) Dynamics of proteins predicted by molecular dynamics simulations and analytical approaches: application to α-amylase inhibitor. *Proteins* **40,** 512–524
44. Chovancova, E., Pavelka, A., Benes, P., Strnad, O., Brezovsky, J., Kozlikova, B., Gora, A., Sustr, V., Klvana, M., Medek, P., Biedermannova, L., Sochor, J., and Damborsky, J. (2012) CAVER 3.0: a tool for the analysis of transport pathways in dynamic protein structures. *PLoS Comput. Biol.* **8,** e1002708
45. Delano, W. L. (2011) The PyMOL Molecular Graphics System, version 1.5.0.4, Schrödinger, LLC, New York
46. Laskowski, R. A., and Swindells, M. B. (2011) LigPlot+: multiple ligand-protein interaction diagrams for drug discovery. *J. Chem. Inf. Model.* **51,** 2778–2786
47. Kumari, R., Kumar, R., Open Source Drug Discovery Consortium, and Lynn, A. (2014) g-mmpbsa: a GROMACS tool for high-throughput MM-PBSA calculations. *J. Chem. Inf. Model.* **54,** 1951–1962
48. Baker, N. A., Sept, D., Joseph, S., Holst, M. J., and McCammon, J. A. (2001) Electrostatics of nanosystems: application to microtubules and the ribosome. *Proc. Natl. Acad. Sci. U.S.A.* **98,** 10037–10041

Structural Plasticity of Cholesteryl Ester Transfer Protein Assists the Lipid Transfer Activity

Venkat R. Chirasani, Prasanna D. Revanasiddappa and Sanjib Senapati

J. Biol. Chem. 2016, 291:19462-19473.
doi: 10.1074/jbc.M116.744623 originally published online July 20, 2016